JOURNAL OF SOLID STATE CHEMISTRY 45, 71–79 (1982)

Structure Determination of $CaMnO_3$ and $CaMnO_{2.5}$ by X-Ray and Neutron Methods*

K. R. POEPPELMEIER, M. E. LEONOWICZ, J. C. SCANLON, AND J. M. LONGO

Exxon Research and Engineering Company, P.O. Box 45, Linden, New Jersey 07036

AND W. B. YELON

University of Missouri, Columbia, Missouri 65201

Received April 28, 1982

Low-temperature synthesis of the oxygen-deficient compound $CaMnO_{2.5}$ from polycrystalline $CaMnO_3$ preserves the existing structural framework of the oxidized precursor. The crystal structure of $CaMnO_{2.5}$ was determined using neutron powder diffraction data analyzed by the Reitveld profile refinement method. The structure of the reduced phase can be described by the orthorhombic distortion $(a_0 + b_0/2)/2 = a_c\,2^{1/2}$, where a_c is the simple cubic distance (~3.7 Å) characteristic of the Mn^{4+}–O^{2-}–Mn^{4+} framework in $CaMnO_3$. The unique features of the structure are five-coordinate Mn^{3+} cations with nearly square pyramidal ($\sim C_{4v}$) coordination and ordered oxygen vacancies. The preparation, structure refinement, and noncubic distortions of single crystals of $CaMnO_3$ are also described. Attempts to transform single crystals of $CaMnO_3$ into $CaMnO_{2.5}$ by well-ordered topotactic changes have not been successful.

Introduction

When crystalline solids undergo chemical reactions that preserve the crystallographic orientation of the physical sample, there may be some three-dimensional correspondence between the structures of the product and the starting material. Successful syntheses of this kind are usually performed under carefully controlled and prescribed conditions. In a previous paper (*1*), the preparation of the perovskite-related compound $CaMnO_{2.5}$ in polycrystalline form by reduction at low temperatures was described. Unfortunately, repeated attempts to transform individual single crystals of $CaMnO_3$ into single crystals of $CaMnO_{2.5}$ by well-ordered topotactic changes have resulted only in crystallites with random orientations. Nonetheless, while the failure to effect this topotactic transformation leaves several important structural questions unresolved, it has been possible using powder neutron diffraction data analyzed by the Reitveld profile refinement (*2*) technique to verify the oxygen vacancy ordering and

* Presented at the Symposium on the Electronic Structure and Bonding in Solids, 183rd National Meeting, American Chemical Society, held in Las Vegas, Nevada, March 30–31, 1982.

0022-4596/82/130071-09$02.00/0

corresponding square pyramidal coordination ($\sim C_{4v}$) of manganese previously proposed (*1*) for $CaMnO_{2.5}$. The site preference of Mn^{3+} (d^4) in part determines the oxygen vacancy distribution, and similar manganese–oxygen vacancy pairs may be expected to influence the stacking sequence of other manganese perovskites. The preparation, structure refinement, and noncubic distortions of the $CaMnO_3$ single crystals prepared for the topotactic transformation experiments are also described.

Experimental Procedures and Results

Sample Preparation

Single crystals of $CaMnO_3$ ranging up to 0.5 mm maximum dimension were grown from a flux of calcium chloride saturated with 7 mole% calcium oxide. Polycrystalline $CaMnO_3$ was prepared from the calcite precursor $CaMn(CO_3)_2$ by oxidative decomposition (*3*) at 1000°C in air, added to the flux mixture, and heated to 900°C for several days in an open platinum crucible. The sample was cooled slowly through the eutectic of the CaO–$CaCl_2$ system (*4*) to 700°C, and then to room temperature more rapidly. The crystals were separated from the flux by a water wash. Exsolution of calcium oxide from $CaMnO_3$ to form $CaMn_2O_4$ (*3*) occurred if it was not added to the $CaCl_2$ flux. When more than 7 mole% calcium oxide was used, the excess reacted with $CaMnO_3$ to form crystals of Ca_2MnO_4. There was no evidence for the intermediate compounds $Ca_3Mn_2O_7$ (*3*) or $Ca_4Mn_3O_{10}$ (*3*) in the latter case.

Earlier work with polycrystalline $CaMnO_3$ (*1*) had shown that the oxygen-deficient phase $CaMnO_{2.5}$ could be prepared through the reaction

$$CaMnO_3(s) \xrightarrow[300°C]{H_2} CaMnO_{2.5} \xrightarrow[325°C]{H_2} CaMnO_2 \quad (1)$$

in the narrow temperature range 300–325°C in hydrogen. When crystals of $CaMnO_3$ were subjected for 24 hr to 10% H_2/He at 300°C they were transformed into a polycrystalline state, even though their exterior physical appearance was unaltered. Consequently, present structural studies have been limited to polycrystalline samples. The $CaMnO_{2.5}$ used in the powder neutron diffraction study was prepared according to Eq. (1).

After calcination of the calcite precursor $CaMn(CO_3)_2$, unreacted carbonate precursor could not be detected in the powder X-ray diffraction pattern or infrared spectrum of the polycrystalline $CaMnO_3$ used in these studies. The identification of polycrystalline and single-crystal $CaMnO_3$ was confirmed by comparison with the cell parameters reported in the literature (*5*). Oxygen content of the oxidized and more reduced compositions in Eq. (1) was established by hydrogen reduction using a Fisher thermogravimetric analyzer equipped with a Cahn electrobalance. When weight loss was attributed to manganese with an oxidation state greater than two, their compositions were determined to be within one atomic% oxygen of the theoretical values $CaMnO_{3.00}$, $CaMnO_{2.50}$, and $CaMnO_{2.00}$.

Data Collection and Structure Refinement of $CaMnO_3$

A small single crystal of equidimension (0.15 mm) was used for the structure determination. A summary of the crystal data and refinement results is given in Table I. The lattice parameters were refined from 25 reflections automatically centered on an Enraf–Nonius CAD-4 diffractometer using graphite-monochromatized Mo$K\alpha$ (λ = 0.71073 Å) radiation. Data were collected using the diffractometer in θ–2θ scan mode where the scan rate was varied between 2 and 13° 2θ min^{-1} and the scan range was 1.8° 2θ plus a systematic allowance for

TABLE I

CRYSTALLOGRAPHIC DATA FOR $CaMnO_3$

Formula	$CaMnO_3$
Z	4
Density (calc)	4.59
Space group	*Pnma*
Lattice constants (Å)	
a	5.279(1)
b	7.448(1)
c	5.264(1)
V (Å^3)	207.0(1)
Unique data	
No. examined	1618
No. observed	1104
Extinction (g)	1.23×10^{-5}
Refinement	
R_1	0.039
R_2	0.045
ESD (unit wt)	1.16
Data/parameters	38.1

spectral dispersion. Diffracted intensities and their associated estimated standard deviations were computed from the formulae $I = S(C - RB)$ and $\sigma(I) = [S^2(C + R^2 B) + (kI)^2]^{1/2}$, where C is the total count recorded during the scan, $R = 2.0$ is the ratio of scanning time to the total background B, S is the scan rate, and $k = 0.05$ is a factor introduced to reflect instrument instability. From these data the structure factors and their estimated standard deviations were computed by using $|F_0| = (I/Lp)^{1/2}$ and $\sigma(F_0) = \sigma(I)/2|F_0|Lp$, where L and p are the Lorentz and polarization corrections. Corrections for the absorption of X-rays were not made. Three reflections periodically monitored during the data collection displayed insignificant intensity variations.

The structure was refined using the full-matrix least-squares program in the Enraf–Nonius SDP package of programs, an integrated set of crystallographic programs for PDP-11 series computers. The quantity minimized in the least squares was $\Sigma w(|F_0| - |F_c|)^2$, with $w = \sigma(F_0)^{-2}$ with $\sigma(F_0)$ defined above. The definition of the weighted residual is $R_2 = [\Sigma w(|F_0| - |F_c|)^2 / \Sigma w|F_0|^2]^{1/2}$ and the form of the extinction correction applied was $(1 + gI_c)^{-1}$. The space group ambiguity was eliminated by refinement of the structure in the equivalent noncentrosymmetric group $Pn2_1a$ (No. 33, $Pna2_1$), but these calculations led to insignificant residual reduction as judged by Hamilton's test (*6*). The final difference Fourier synthesis displayed uniform background density throughout the unit cell. A listing of $|F_{obs}|$ and $|F_{calc}|$ values is provided as supplementary material.[1] Tables II and III list the refined structural parameters and bond distances, respectively. Figure 1a is an ORTEP drawing of the structure.

Data Collection and Structure Refinement of $CaMnO_{2.5}$

Neutron powder data were obtained at the Missouri University Research Reactor (MURR) using neutrons with wavelength 1.293 Å on a 10-g sample tightly compressed in a vanadium cylinder. Since magnetic susceptibility measurements (*1*) for $CaMnO_{2.5}$ over the range 80–600K showed magnetic behavior with an ordering temperature T_c near 350K, data were collected at room temperature and 120°C. Spectra were recorded by step scanning in 0.1° increments in 2θ over the angular range $5° < 2\theta < 100°$ on a two-axis diffractometer. The higher-temperature scan was collected in order to confirm that those reflections in the room-temperature scan which could not be indexed on the chemical cell were magnetic

[1] See NAPS document No. 03998 for 5 pages of supplementary material. Order from ASIS/NAPS, Microfiche Publications, P.O. Box 3513, Grand Central Station, New York, N.Y. 10163. Remit in advance $4.00 for microfiche copy or for photocopy, $7.75 for up to 20 pages plus $.30 for each additional page. All orders must be prepaid. Institutions and organizations may order by purchase order. However, there is a billing and handling charge for this service of $15. Foreign orders add $4.50 for postage and handling, for the first 20 pages, add $1.00 for additional 10 pages of material. Remit $1.50 for postage of any microfiche orders.

TABLE II

REFINED POSITIONAL AND THERMAL PARAMETERS[a] IN $CaMnO_3$

Atom	Site	Symmetry	x	y	z
Ca	4*c*	*m*	0.03331(7)	0.25000	−0.00569(8)
Mn	4*b*	$\bar{1}$	0.00000	0.00000	0.50000
O(1)	4*c*	*m*	0.48986(30)	0.25000	0.06593(31)
O(2)	8*d*	1	0.28728(19)	0.03358(16)	−0.28789(18)

	β_{11}	β_{22}	β_{33}	β_{12}	β_{13}	β_{23}
Ca	0.00388(8)	0.00208(3)	0.00394(6)	0.00000	−0.00146(16)	0.00000
Mn	0.00130(4)	0.00095(2)	0.00164(4)	0.00001(4)	−0.00015(11)	−0.00011(7)
O(1)	0.00585(32)	0.00093(12)	0.00460(28)	0.00000	−0.00058(52)	0.00000
O(2)	0.00294(16)	0.00246(10)	0.00315(15)	−0.00086(26)	−0.00324(31)	0.00058(25)

[a] The general form of the anisotropic thermal ellipsoid is $\exp[-(\beta_{11}h^2 + \beta_{22}k^2 + \beta_{33}l^2 + \beta_{12}hk + \beta_{13}hl + \beta_{23}kl)]$.

TABLE III

SELECTED DISTANCES (Å) AND ANGLES (°) IN $CaMnO_3$

Ca–O(1)	2.326[a]	$x - \frac{1}{2}$	$\frac{1}{2} - y$	$\frac{1}{2} - z$[b]
	2.439	x	y	z
	2.894	$x - 1$	y	z
	2.958	$x - \frac{1}{2}$	$\frac{1}{2} - y$	$-\frac{1}{2} - z$
Ca–O(2)	2.338	$x - \frac{1}{2}$	$\frac{1}{2} - y$	$-\frac{1}{2} - z$
	2.338	$x - \frac{1}{2}$	y	$-\frac{1}{2} - z$
	2.570	x	y	z
	2.570	x	$\frac{1}{2} - y$	z
	2.583	$\frac{1}{2} - x$	$\frac{1}{2} + y$	$\frac{1}{2} + z$
	2.583	$\frac{1}{2} - x$	$-y$	$\frac{1}{2} + z$
	3.117	$-x$	$-y$	$-z$
	3.117	$-x$	$\frac{1}{2} + y$	$-z$
Mn–O(1)	1.895	$x - \frac{1}{2}$	$\frac{1}{2} - y$	$\frac{1}{2} - z$
	1.895	$\frac{1}{2} - x$	$y - \frac{1}{2}$	$\frac{1}{2} + z$
Mn–O(2)	1.900	x	y	$z + 1$
	1.900	$-x$	$-y$	$-z$
	1.903	$\frac{1}{2} - x$	$-y$	$\frac{1}{2} + z$
	1.903	$x - \frac{1}{2}$	y	$\frac{1}{2} - z$
O(1)–Mn–O(1)	180.0[a]			
O(1)–Mn–O(2)	90.1 (89.9)			
	90.0 (90.0)			
O(2)–Mn–O(2)	180.0			
	90.8 (89.2)			
Mn–O(1)–Mn	158.6			
Mn–O(2)–Mn	157.2			

[a] The estimated standard deviation is (1) in the last decimal place.

[b] Symmetry operation used to generate the oxygen coordinates from those given in Table II.

in origin. Two strong reflections ($01\frac{1}{2}$) and ($11\frac{1}{2}$), along with a weak ($21\frac{1}{2}$) reflection, were observed to be of magnetic origin and were excluded from the refinement of the room-temperature data. All other reflections in the pattern could be indexed on the chemical cell with the orthorhombic cell parameters $a = 5.424(2)$, $b = 10.230(4)$, and $c = 3.735(2)$ Å and showed no recognizable magnetic contribution. The room-temperature data were refined using the Reitveld profile analysis method (*2*) starting with the model proposed earlier (*1*) in the refinement of powder X-ray data. The ideal atomic positions for $CaMnO_{2.5}$, space group *Pbam*, used as starting positions were: 4 Ca in (h), $x \simeq \frac{1}{4}$, $y \simeq \frac{3}{8}$, $z = \frac{1}{2}$; 4 O(1) in (h), $x \simeq \frac{1}{4}$, $y \simeq \frac{1}{8}$, $z = \frac{1}{2}$; 4 Mn in (g), $x \simeq \frac{1}{4}$, $y \simeq \frac{1}{8}$, $z = 0$; 4 O(2) in (g), $x \simeq 0$, $y \simeq \frac{1}{4}$, $z = 0$; and 2 O(3) in (a), $x = y = z = 0$. The coherent scattering lengths used were $b_{Ca} = 0.47$, $b_{Oxy} = 0.58$ (*7*), and $b_{Mn} = -0.372$ (*8*), all $\times 10^{-12}$ cm. Background contributions to the diffraction pattern were estimated and 21 parameters that included individual positional and isotropic temperature parameters, cell constants, peak width parameters, and a zero-point were refined until all parameter shifts were less than 0.3σ. A profile and weighted profile R factor of 13.3 and 15.3%, to be

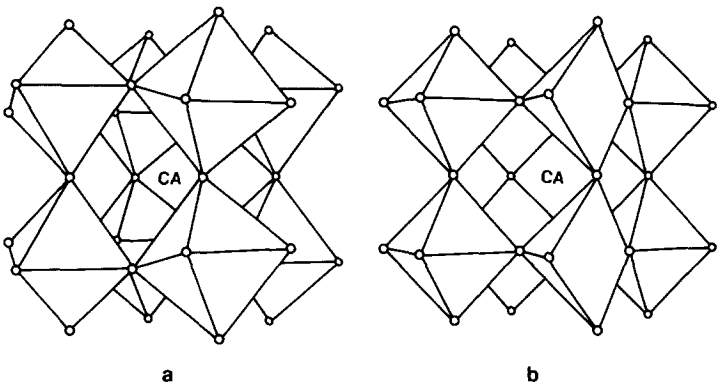

FIG. 1. The $MnO_{6/2}$-connected polyhedra of $CaMnO_3$ (a) and the $MnO_{5/2}$ polyhedra found in $CaMnO_{2.5}$ (b).

compared with a value of 4.7% calculated from the statistical precision of the data, were considered acceptable. The R factor based on integrated intensities was 8.4%. Table IV compares the observed neutron powder diffraction intensities with those calculated from the refined structure. Final positional and thermal parameters and some important bond distances are reported in Table V. Refinement in the noncentrosymmetric group $Pba2$ (No. 32) led to insignificant residual reduction and a negative thermal parameter at the manganese site. Refinement of the neutron data collected at 120°C gave an identical chemical structure with all parameters within 3σ of those described in Table V and no significant improvement of residuals. The refinement with either data set was sensitive to the background parameters used, owing to a high background (see Fig. 2) that was not due simply to incoherent scattering of the vanadium container and sample.[2] The origin of the diffuse scattering and undulating background observed is not completely understood at this time, but it would appear that there is some minor phase(s) present. Future structural studies will require modifications in sample preparation procedures in order to limit competing reactions that produce phases such as $CaMnO_{2.75}$ (incomplete reduction) and $CaMn_2O_4$ (decomposition), while ensuring complete reaction of the starting material.

Discussion

The problem of sample homogeneity encountered during the analysis of the neutron diffraction data discussed above illustrates a prime difficulty with obtaining structural information from polycrystalline samples. Indeed, minor phase contamination of powdered materials is many times aggravated during synthesis when reaction conditions are chosen to be far from the equilibrium values of the product; this is often the case when side reactions must be suppressed. It is clear from a detailed examination of the diffraction pattern that the sample used for the neutron diffraction experiment was inhomogeneous, and this factor, rather than inadequacies in the proposed structure, caused the residuals obtained in the profile refinement to be somewhat high. Furthermore, the fact that

[2] *Note added in proof.* Refinement with the background correction parameterized as a function of angle and a non-Gaussian profile function (D. B. Wiles and R. A. Young, *J. Appl. Cryst.* **14**, 149 (1981)) results in improved figures of merit (R factors R_I = 3.4, R_P = 13.9, R_{WP} = 13.9, and R_E = 5.7) and atomic thermal parameters. However, the refined positional parameters remained essentially at the values in Table V.

TABLE IV

POWDER NEUTRON DIFFRACTION DATA FOR $CaMnO_{2.5}$

hkl	d_{calc}[a]	I_{calc}	I_{obsd}
020	5.115	3.0	3.8
110	4.792	7.4	6.8
001	3.735	11.7	13.0
120	3.721	12.2	14.4
021	3.016	6.6	6.8
111	2.946	6.9	5.3
130	2.887	10.9	10.4
200	2.712	0.2	1.0
121	2.636	25.7	29.0
210	2.621	2.4	2.5
040	2.558	0.7	2.9
220	2.396	0.1	4.7
140	2.313	11.2	11.3
131	2.284	24.4	24.3
201	2.195	94.6	99.4
211	2.146	49.3	52.6
230	2.123	11.5	11.3
041	2.110	102.3	100.0
221	2.017	0.3	2.5
141	1.967	2.9	5.2
150	1.914	0.5	1.4
002	1.868	22.6	24.3
240	1.861	16.6	18.2
231	1.845	0.1	0.1
310	1.781	0.4	0.8
022	1.754	1.0	0.6
112	1.740	2.1	1.9
060	1.705	0.0+	0.0
320	1.705	0.0+	0.0
151	1.704	2.8	2.8
122	1.669	7.2	6.2
241	1.665	9.4	8.1
250	1.633	3.1	2.8
160	1.623	0.4	0.4
311	1.607	0.4	0.4
330	1.597	6.7	7.4
132	1.568	6.7	5.6
061	1.551	1.3	0.2
321	1.551	0.8	0.1
202	1.538	0.8	0.2

[a] Calculated with $a = 5.424$, $b = 10.230$, $c = 3.735$ Å; $0kl$, $k \neq 2n$ and $h0l$, $h \neq 2n$ are forbidden reflections.

TABLE V

ATOM PARAMETERS, BOND DISTANCES, AND ANGLES FOR $CaMnO_{2.5}$[a,b]

Atom	Site	*x*	*y*	*z*	*B* (Å²)
Ca	4*h*	0.2990(16)	0.3610(10)	½	1.2(2)
O(1)	4*h*	0.2875(17)	0.1027(9)	½	2.8(3)
Mn	4*g*	0.2826(22)	0.1201(11)	0	0.3(2)
O(2)	4*g*	0.0800(13)	0.2824(8)	0	0.1(2)
O(3)	2*a*	0	0	0	0.4(2)

Selected bond distances (Å) and angles (°)

Mn–O(1)	1.876(2) [2×][c]	Ca–O(2)	2.355(7)
Mn–O(2)	1.991(14) [1×]	Ca–O(2a)	2.822(9)
Mn–O(2a)	1.897(14) [1×]	Ca–O(3a)	2.588(7)
Mn–O(3)	1.964(12) [1×]	Ca–O(1)	2.643(14)
		Ca–O(1a)	2.676(11)
O(3)–Mn–O(2)	95.2(6)	Ca–O(1b)	2.517(14)
O(3)–Mn–O(1)	87.2(4)	Ca–O(1c)	2.799(11)
O(2)–Mn–O(2a)	91.8(6)		
O(2)–Mn–O(1)	95.0(4)	Mn(1)–Mn(1a)	3.406(16)
O(2a)–Mn–O(1)	92.2(4)	O(1b)–O(1c)	3.119(11)

[a] The errors (in parentheses) refer to one standard deviation.
[b] Lattice constants: $a = 5.424(2)$, $b = 10.230(4)$, $c = 3.735(2)$ Å.
[c] Frequency of occurrence as nearest neighbors of the cation.

both the X-ray (*1*) and neutron refinements, with their differing sensitivities to metal and oxygen atom positions, yield essentially the same structural model lends credence to the description of the manganese–oxygen vacancy pairs presented herein.

Figure 1a is an ORTEP drawing of the structure of $CaMnO_3$ which illustrates the $a^-b^+a^-$ tilt system ($a_p = c_p \neq b_p$, $\beta \neq 90°$) (*9*) that describes the distortion of this material from ideal cubic symmetry. When values of 3.790 Å (twice Mn–O(1)) and 3.803 Å (twice the average Mn–O(2)) are used for the aristotype cell length a_0, one computes tilt angles $a^- = 7.6°$ and $b^+ = 8.6°$. These values can then be used to calculate Mn–O–Mn bond angles of Mn–O(1)–Mn = 158.6° and Mn–O(2)–Mn = 157.1°, assuming rigid body rotations of octahedra. The derived bond angles agree with those determined in the single-crystal analysis (see Table III). These results on $CaMnO_3$ represent the first complete single-crystal determination of this material and there is good agreement between the observed distances and those predicted from the ionic radii of Shannon (*10*), for six-coor-

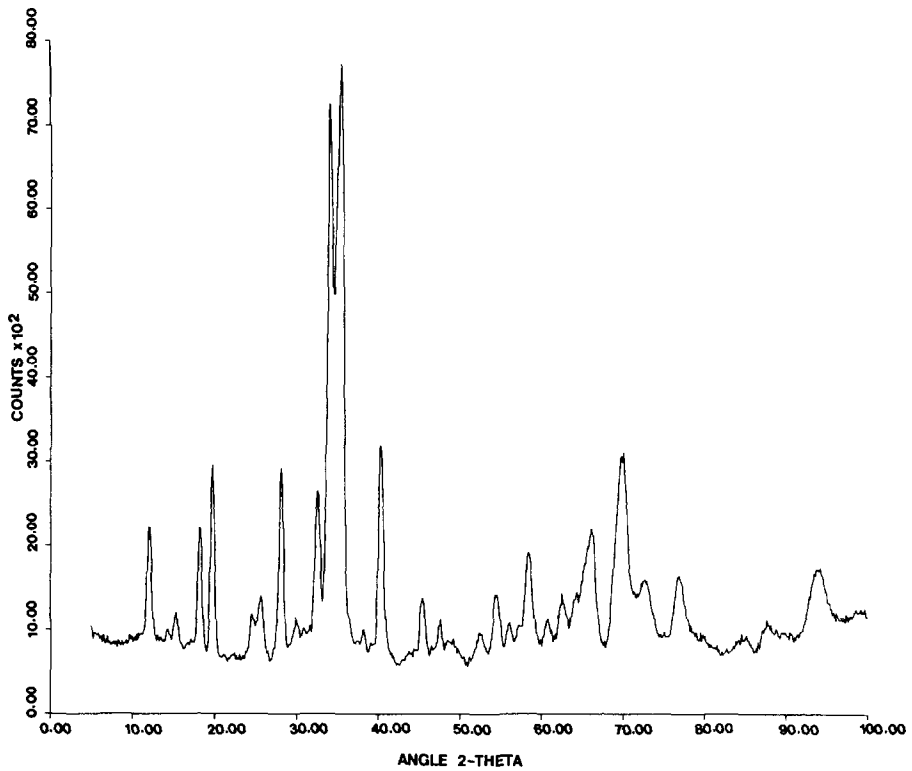

FIG. 2. Neutron powder pattern of $CaMnO_{2.5}$ recorded at room temperature.

dinate Mn^{4+} (0.53 Å) and O^{2-} (1.40 Å), and the average Ca–O distance (2.65 Å) with that predicted (2.72 Å).

Figure 1b illustrates the respective polyhedra in the oxygen-defect phase $CaMnO_{2.5}$. Notice that in $CaMnO_{2.5}$ all the $MnO_{5/2}$ polyhedra remain connected through Mn–O–Mn linkages similar to those in $CaMnO_3$, and that the oxygen vacancies form parallel channels throughout the structure. The oxygen vacancies are generated by the reduction of Mn^{4+} in $CaMnO_3$ to Mn^{3+} in the phase $CaMnO_{2.5}$. In Fig. 3 the ordering pattern of the oxygen vacancies is illustrated in schematic form. The vacancies order in every (001) BX_2 plane of cubic perovskite with alternate $[110]_c$ strings of oxygen atoms (based on the simple 3.7-Å cell) that are missing every other oxygen. The vacancies are displaced by $a_0/2$ in alternate strings. Thus the manganese ions are coordinated by five oxygen anions in $CaMnO_{2.5}$ (see Fig. 1b) as opposed to six in $CaMnO_3$ (Fig. 1a). The structure of the defect phase is shown in more detail in Fig. 4. From this figure, it can be seen that the Mn^{3+} cations have nearly square pyramidal coordination with O–Mn–O bond angles ranging from 87 to 95°. The differentiating electron of high-spin Mn^{3+} occupies the d_{z^2} orbital with the $d_{x^2-y^2}$ orbital on the metal used in metal–oxygen σ bonds and $sp^3d_{x^2-y^2}$ states characteristic of square pyramidal geometry. The unequal occupation of the d_{z^2} and $d_{x^2-y^2}$ orbitals results in a long Mn–O(2) distance of 1.99 Å that is *trans* to the oxygen vacancy. This bond was determined to be the long Mn–O distance of the square pyramid in the X-ray refinement as well. However, some dis-

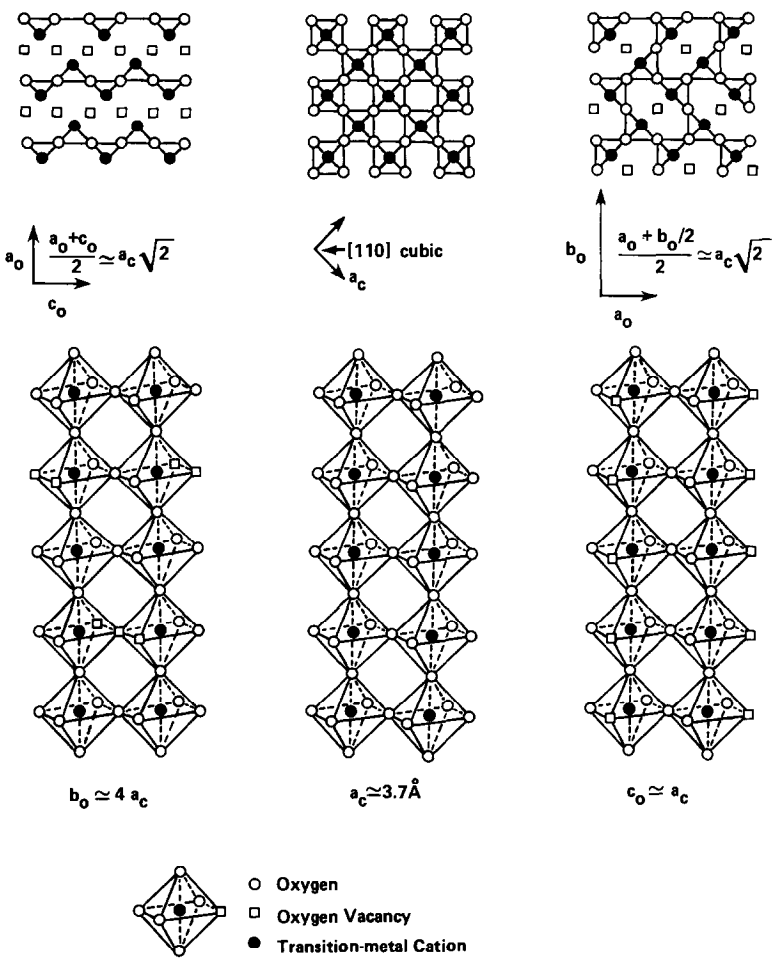

FIG. 3. Schematic structures of a stoichiometric ABO_3 perovskite (center), $ABO_{2.5}$ brownmillerite (left), and $CaMnO_{2.5}$ (right).

crepancies exist between this study and the X-ray refinement (*1*) in Mn–O bond distances. In particular, the X-ray refinement indicated that O(2) formed a long 2.09-Å and a short 1.80-Å oxygen–manganese bond, whereas the neutron study has calculated these distances to be 1.99 and 1.90 Å, respectively. The values reported herein are probably closer to the true values, since large errors associated with these distances in the X-ray study (*1*) were indicated.

The coordination by oxygen of the Ca^{2+} cations, as depicted in Fig. 4, has changed from 12 (4 + 4 + 4) in $CaMnO_3$ to 10 (3 + 4 + 3) in $CaMnO_{2.5}$ due to the oxygen vacancies. The polyhedron around the calcium cation is a distorted tricapped trigonal prism with an additional more distant oxygen. Two of the three prism faces remain capped much as they were in the oxidized form, while the calcium cation attracts O(1b) at 2.52 Å more strongly than O(1c) at 2.80 Å through the third face of the prism. The calcium cations appear to play a secondary role in maintaining parallel channels of oxygen vacancies which may account for the low activation barriers to reoxidation of $CaMnO_{2.5}$ observed (*1*).

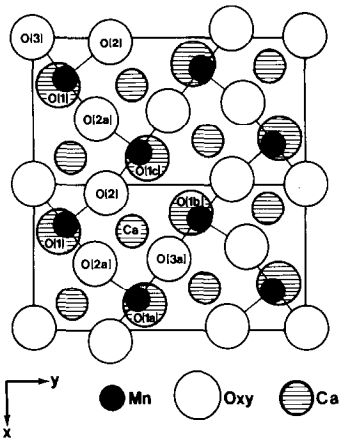

FIG. 4. The projection down the c axis of the $CaMnO_{2.5}$ structure. Atoms are at $z = 0$ (open and solid circles) or $z = \frac{1}{2}$ (hatched circles).

Conclusions

The preparation of $CaMnO_{2.5}$ by low-temperature reduction of polycrystalline $CaMnO_3$ results in powder X-ray (*1*) and neutron diffraction patterns with sufficient detail to justify the selection of a unit cell wherein the oxygen vacancies can be ordered. We show that the distribution of oxygen vacancies in $CaMnO_{2.5}$ is a consequence of the square pyramidal coordination of Mn^{3+}, although trigonal bipyramidal coordination with Mn^{3+} covalently bonded to two axial oxygen atoms might have been expected (*11*, *12*). This early work showed conclusively that the many polytypes which had been observed for $AMnO_3$ (A = Sr, Ba) were associated with the method of preparation and therefore their oxygen deficiency. Although it has been determined in $Ba_{0.5}Sr_{0.5}MnO_{2.84}$ (*13*) that the oxygen vacancies are distributed in hexagonal AO_{3-x} layers (that is, face-shared positions between octahedra) and that oxygen sites in cubic layers (or between corner-linked octahedra) are fully occupied, we suggest that the introduction of manganese–oxygen vacancy pairs in the multilayer compounds $BaMnO_{3-x}$ and $SrMnO_{3-x}$ may occur as it does in $CaMnO_{2.5}$ to the extent $AO_{2.5}$ planes can form from AO_3 layers of cubic close-packing symmetry.

Acknowledgments

The authors express their thanks to Mr. J. Dunn for the preparation of samples and to Dr. A. J. Jacobson for his helpful comments on profile analysis.

References

1. K. R. POEPPELMEIER, M. E. LEONOWICZ, AND J. M. LONGO, *J. Solid State Chem.* **44**, 89 (1982).
2. H. M. RIETVELD, *Acta Crystallogr.* **22**, 151 (1967).
3. H. S. HOROWITZ AND J. M. LONGO, *Mater. Res. Bull.* **13**, 1359 (1978).
4. D. A. WENZ, I. JOHNSON, AND R. D. WOLSON, *J. Chem. Eng. Data* **14**, 252 (1969).
5. J. B. MACCHESNEY, H. J. WILLIAMS, J. F. POTTER, AND R. C. SHERWOOD, *Phys. Rev.* **164**, 779 (1967).
6. W. C. HAMILTON, *Acta Crystallogr.* **18**, 502 (1965).
7. G. E. BACON, "Neutron Diffraction," 3rd ed., p. 39, Oxford Univ. Press (Clarendon), London/New York (1975).
8. A. J. JACOBSON, B. C. TOFIELD, AND B. E. F. FENDER, *J. Phys. C Solid State Phys.* **6**, 1615 (1973).
9. A. M. GLAZER, *Acta Crystallogr. Sect. B* **28**, 3384 (1972); *Sect. A* **31**, 756 (1975). The distortion described in the present report and shown in Fig. 1a is relative to the standard group setting *Pnma*, and would be described as $a^+b^-b^-$ ($a_p \neq b_p = c_p, \alpha \neq 90°$), space group *Pmnb*, in Glazer's nonstandard nomenclature.
10. R. D. SHANNON, *Acta Crystallogr. Sect. A* **32**, 751 (1976).
11. T. NEGAS AND R. S. ROTH, *J. Solid State Chem.* **1**, 409 (1970).
12. T. NEGAS AND R. S. ROTH, *J. Solid State Chem.* **3**, 323 (1971).
13. A. J. JACOBSON AND A. J. W. HORROX, *Acta Crystallogr. Sect. B* **32**, 1003 (1976).